Three-dimensional image reconstruction from exponential parallel-beam projections

Jean-Marc Wagner, Frédéric Noo

Abstract— **In this paper, we present an FBP algorithm suitable for image reconstruction from exponential X-ray (parallel-beam) projections sampled on any subset of the sphere that includes great circles. This algorithm is similar to the TTR-algorithm of Ra *et al.* (1982) for non-attenuated projections. It is derived by combining all reconstructions that can be obtained from subsets of measurements corresponding to great circles. Our results generalize those published by I. Hazou (1988) and Weng *et al.* (1996) for reconstruction from projections sampled on the unit sphere. However, they remain modest as they only apply to specific sets of measurements.**

Keywords— **attenuation, parallel-beam projections, 3D reconstruction.**

I. Introduction

This work presents new mathematical results concerning three-dimensional (3-D) image reconstruction from exponential X-ray (parallel-beam) projections.

The exponential X-ray transform is a mathematical tool useful in SPECT imaging and also in Intensity Modulated Radiation Therapy [1]. In 2-D SPECT, it is the basis for the development of fast analytical reconstruction methods with accurate correction for attenuation and depth-dependent collimator-response [2], [3]. In fully 3-D SPECT, it provides a way to perform accurate attenuation correction without transmission measurements [4], which is highly attractive for sophisticated imaging systems such as the Rotating-Slant-Hole scanner [5].

2-D image reconstruction from exponential X-ray projections has been widely studied over the last twenty years and is now well-understood, especially thanks to the significant work of Pan and Metz [6], [7]. In fully 3-D geometry, the situation is quite different. To our knowledge, only two works concerning exact 3-D reconstruction from exponential X-ray projections have been published so far. These two works (see [8] and [9]) assume both that the projections are finely sampled on the unit sphere. It is currently unknown if exact reconstruction can be achieved from more general data sets, such as those satisfying Orlov's condition for reconstruction in the non-attenuated case [10]. Such a question is mathematically difficult to answer because 3-D reconstruction theory for non-attenuated X-ray projections [11] is not readily modified to handle exponential X-ray projections.

In this paper, we present a closed-form inversion formula for image reconstruction from exponential X-ray projections sampled on any subset of the unit sphere that includes great circles. A basic example of such a subset is the equatorial band illustrated in figure 1a. Although unusual, we note that this data acquisition geometry could be easily implemented on existing SPECT scanners.

J.-M Wagner and F. Noo are with the Electricity Montefiore Institute, University of Liege, Belgium. E-mail: wagner@montefiore.ulg.ac.be.

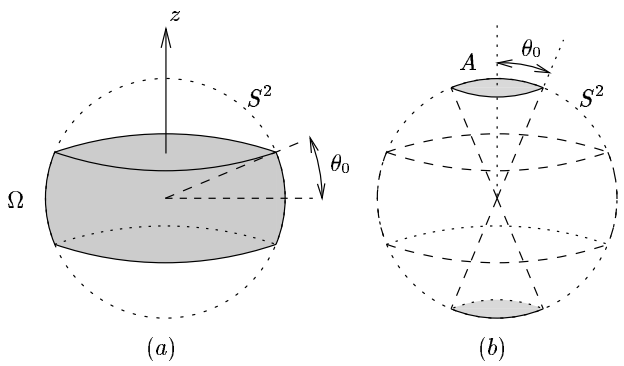

Fig. 1. (a) Description of the equatorial band Ω (b) Description of the set A.

The derivation of our formula follows the same lines as the work of Ra *et al.* [12] for image reconstruction from non-attenuated projections. From the theory for the 2-D Radon transform, Ra *et al.* derived the first True Three-dimensional Reconstruction (TTR) algorithm for non-attenuated X-ray projections. From the theory for the 2-D exponential Radon transform, we have derived a true 3-D reconstruction algorithm for exponential X-ray projections. This algorithm, called the A-TTR algorithm, where A stands for "attenuated", processes the data in a filtered-backprojection (FBP) way.

Our results generalize those published by Hazou [8] and Weng *et al.* [9] for projections sampled on the full sphere. However, they remain modest as they only apply to specific sets of measurements - those including great circles. We believe that our work is one step further towards full understanding of the 3-D exponential X-ray transform.

This paper comprises four sections. Section II gives a general description of the A-TTR algorithm and provides mathematical details of its derivation. Section III concerns applications of the A-TTR algorithm to particular geometries ; we investigate the full sphere and the equatorial band geometries. Conclusions are given with a short discussion in section IV.

II. A-TTR ALGORITHM

A. Notations

The data used for reconstruction are exponential X-ray projections

$$p(\underline{\theta},\underline{s}) = \int_{-\infty}^{+\infty} dt\, f(\underline{s}+t\,\underline{\theta})\, e^{\mu_0 t}, \qquad \underline{s}\cdot\underline{\theta}=0 \qquad (1)$$

"measured" for a set of directions $\underline{\theta}$ on the unit sphere. The 3-D image to be reconstructed is f and μ_0 is the attenuation coefficient. Vector $\underline{s}$ is orthogonal to $\underline{\theta}$ and is used to specify different lines of integration in the direction $\underline{\theta}$. See figure 2. We assume that the projections are complete, i.e. that $p(\underline{\theta},\underline{s})$ is known for all $\underline{s}$ orthogonal to $\underline{\theta}$.

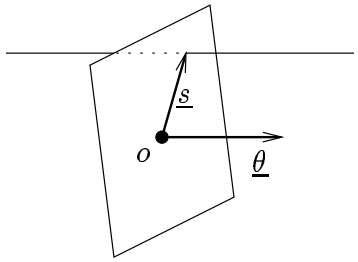

Fig. 2. Description of the projections: $\underline{s}$ is used to specify different lines of integration in the direction $\underline{\theta}$, 0 is the origin of the image space.

Technically speaking, there exist no scanners which directly provide exponential X-ray projections. However, to symplify the exposition we will assume that exponential X-ray projections can be directly measured. In SPECT, exponential X-ray projections are obtained from the measured attenuated projections when the attenuation coefficients are constant in the emission region [13].

If a detector with pixels of coordinates (u,v) oriented along unit orthogonal vectors $\underline{\alpha}$ and $\underline{\beta}$ perpendicular to $\underline{\theta}$ is used to measure $p(\underline{\theta},\underline{s})$, one can write

$$\underline{s} = u\,\underline{\alpha} + v\,\underline{\beta}, \qquad u\in\mathbb{R}, \quad v\in\mathbb{R} \qquad (2)$$

and

$$p(\underline{\theta},\underline{s}) = p_D(\underline{\theta},u,v) = \int_{-\infty}^{+\infty} dt\, f(u\,\underline{\alpha}+v\,\underline{\beta}+t\,\underline{\theta})\, e^{\mu_0 t}\,. \quad (3)$$

The set of directions $\underline{\theta}$ for which $p(\underline{\theta},\underline{s})$ is known is denoted Ω. We assume that Ω is symmetric (i.e. if $\underline{\theta}\in\Omega$, then $-\underline{\theta}\in\Omega$) and contains great circles. A great circle is the set of unit vectors which are orthogonal to a given direction. We use the notation $\mathcal{C}(\underline{n})$ to describe the great circle of unit vectors orthogonal to $\underline{n}$. The set of vectors $\underline{n}$ corresponding to all great circles in Ω is denoted A. Note that A is symmetric. See figure 1b for an illustration of A for the equatorial band.

It is important to note that any great circle defines a complete set of projections from which exact reconstruction of f is possible. When Ω includes more than one great circle, the data $p(\underline{\theta},\underline{s})$ are therefore redundant. In principle, the reconstruction from data on Ω could be carried out by applying any 2-D reconstruction formula to a number of great circles in Ω and by averaging the different results so obtained. Such an approach is however difficult to implement in practice due to finite sampling considerations. The algorithm presented hereafter presents the advantage of being a fully 3-D reconstruction method. Moreover, it shows that a closed-form inversion formula can be derived for image reconstruction from exponential X-ray projections sampled on more practical sets than the full unit sphere.

B. Algorithm description

The A-TTR algorithm is an FBP algorithm which provides exact reconstruction of f according to the backprojection formula

$$f(\underline{x}) = \int_{\Omega} d\underline{\theta}\; e^{-\mu_0\,\underline{x}\cdot\underline{\theta}}\, p^F\big(\underline{\theta},\underline{x}-(\underline{x}\cdot\underline{\theta})\,\underline{\theta}\big) \qquad (4)$$

where $p^F(\underline{\theta},\underline{s})$ is obtained from $p(\underline{\theta},\underline{s})$ by 2-D convolution:

$$p^F(\underline{\theta},\underline{s}) = \int_{\underline{s}'\cdot\underline{\theta}=0} d\underline{s}'\, p(\underline{\theta},\underline{s}-\underline{s}')\, h(\underline{\theta},\underline{s}')\,. \qquad (5)$$

The convolution filter h is given by

$$h(\underline{\theta},\underline{s}) = \begin{cases} 2\,c\,\dfrac{k_\mu(||\underline{s}||)}{||\underline{s}||}\, w\Big(\underline{\theta}\times\dfrac{\underline{s}}{||\underline{s}||}\Big) & \text{if} \quad \underline{\theta}\times\dfrac{\underline{s}}{||\underline{s}||}\in A \\ \\ 0 & \text{otherwise} \end{cases} \qquad (6)$$

where the symbol $\times$ denotes a cross product, w can be any even positive function defined on the unit sphere ($w(-\underline{n}) = w(\underline{n})$),

$$c = 1/\int_A d\underline{n}\, w(\underline{n})\,, \qquad (7)$$

and k_μ is the notch filter used in FBP inversion of the 2-D exponential Radon transform:

$$\begin{aligned} k_\mu(r) &= \int_{|\nu|>\mu_0/2\pi} d\nu\, \frac{|\nu|}{2}\, e^{j2\pi r\nu} \\ &= -\frac{\cos(\mu_0 r)+\mu_0 r\sin(\mu_0 r)}{4\,\pi^2\, r^2}\,. \end{aligned} \qquad (8)$$

The arbitrary definition of $w(\underline{n})$ in the above equations shows that there exist in general an infinite number of filtered-backprojection formulas for reconstruction from projections sampled on Ω. This property is a consequence of the data redundancy. As in the non-attenuated case [11], different definitions for $w(\underline{n})$ are likely to yield a different image quality in the presence of data noise. The effects of $w(\underline{n})$ on noisy data will however not be analyzed in this paper. In section III, $w(\underline{n})=1$ will be selected, which corresponds to giving the same weight to all great circles of data in Ω.

As readily observed from its definition, the filter h is a generalized function with singularities at $\underline{s}=0$. The implementation of equation (5) therefore requires the use of some

regularization technique. For an accurate computation of $p^F(\underline{\theta},\underline{s})$ from samples of $p(\underline{\theta},\underline{s})$ on a Cartesian grid, we recommend the implementation of (5) in the Fourier domain with some apodizing frequency window, like the Hanning window. Such an implementation requires the knowledge of the Fourier transform of the filter h. We show in the next section that this transform is

$$\begin{aligned} H(\underline{\theta},\underline{\nu}) = & \int_{\underline{s}\cdot\underline{\theta}=0} d\underline{s}\, e^{-j2\pi\underline{s}\cdot\underline{\nu}}\, h(\underline{\theta},\underline{s}) \\ = & \frac{c}{2}\int_{\mathcal{C}^*(\underline{\theta})\cap A} d\underline{n}\, w(\underline{n})\, |\underline{\nu}\cdot(\underline{n}\times\underline{\theta})|\,, \qquad \underline{\nu}\cdot\underline{\theta}=0 \end{aligned} \tag{9}$$

where $\mathcal{C}^*(\underline{\theta})$ is a subset of the great circle $\mathcal{C}(\underline{\theta})$:

$$\mathcal{C}^*(\underline{\theta}) = \mathcal{C}(\underline{\theta}) \setminus \left\{\underline{n}\in\mathcal{C}(\underline{\theta}) \;:\; |\underline{\nu}\cdot(\underline{n}\times\underline{\theta})| < \mu_0/2\pi\right\}. \tag{10}$$

Note, in particular, that $\mathcal{C}^*(\underline{\theta})=\emptyset$ when $||\underline{\nu}|| < \mu_0/2\pi$ because $|\underline{\nu}\cdot(\underline{n}\times\underline{\theta})| < \mu_0/2\pi$ for any $\underline{n}$ in this case. Therefore,

$$H(\underline{\theta},\underline{\nu}) = 0 \quad \text{if} \quad ||\underline{\nu}|| < \mu_0/2\pi. \tag{11}$$

C. Algorithm derivation

This section may be skipped at first reading. Section III provides details on the application of formulas in section II.B to specific geometries.

To derive the A-TTR algorithm, note that exact reconstruction of f is possible from data on any great circle $\mathcal{C}(\underline{n})$ in Ω. Such a reconstruction can be achieved by splitting the reconstruction volume into a set of slices orthogonal to $\underline{n}$ and applying a conventional 2-D algorithm for reconstruction of each slice. Using the 2-D FBP reconstruction formula of Tretiak and Metz [14], one gets the following expression for $f(\underline{x})$ from data on $\mathcal{C}(\underline{n})$: let $\underline{\alpha}=\underline{n}\times\underline{\theta}$ and $\underline{\beta}=\underline{n}$ be the detector axes used to describe $p(\underline{\theta},\underline{s})$, then:

$$f(\underline{x}) \equiv f(\underline{x},\underline{n}) = \int_{\mathcal{C}(\underline{n})} d\underline{\theta}\; e^{-\mu_0\,\underline{x}\cdot\underline{\theta}}\; p_D^F(\underline{\theta},\underline{x}\cdot\underline{\alpha},\underline{x}\cdot\underline{\beta}) \tag{12}$$

where

$$p_D^F(\underline{\theta},u,v) = \int_{\mathbb{R}^2} du'\,dv'\, p_D(\underline{\theta},u-u',v-v')\,\delta(v')\,k_\mu(u')\,. \tag{13}$$

With detector-independent notations, the filtering step of equation (13) is rewritten as

$$p^F(\underline{\theta},\underline{s}) = \int_{\underline{s}'\cdot\underline{\theta}=0} d\underline{s}'\, p(\underline{\theta},\underline{s}-\underline{s}')\,\delta(\underline{s}'\cdot\underline{n})\,k_\mu(\underline{s}'\cdot\underline{\alpha}) \tag{14}$$

and

$$\begin{aligned} f(\underline{x},\underline{n}) &= \int_{\mathcal{C}(\underline{n})} d\underline{\theta}\; e^{-\mu_0\,\underline{x}\cdot\underline{\theta}}\; p_D^F\left(\underline{\theta},\underline{x}\cdot\underline{\alpha},\underline{x}\cdot\underline{\beta}\right) \\ &= \int_\Omega d\underline{\theta}\;\delta(\underline{\theta}\cdot\underline{n})\; e^{-\mu_0\,\underline{x}\cdot\underline{\theta}}\; p^F\left(\underline{\theta},\underline{x}-(\underline{x}\cdot\underline{\theta})\,\underline{\theta}\right). \end{aligned} \tag{15}$$

since $\mathcal{C}(\underline{n})\subset\Omega$ and $\underline{n}\cdot\underline{\theta}=0$ for $\underline{\theta}\in\mathcal{C}(\underline{n})$.

Conceptually, a reconstruction formula such as (15) can be written for any vector $\underline{n}\in A$. The A-TTR algorithm is obtained by averaging all expressions available for f. One writes

$$f(\underline{x}) = c\int_A d\underline{n}\, w(\underline{n})\, f(\underline{x},\underline{n}) \tag{16}$$

using some even positive function $w(\underline{n})$ and the normalization constant c defined by equation (7). From formulas (14) and (15) for $f(\underline{x},\underline{n})$, one gets then

$$f(\underline{x}) = \int_\Omega d\underline{\theta}\; e^{-\mu_0\,\underline{x}\cdot\underline{\theta}} \int_{\underline{s}\cdot\underline{\theta}=0} d\underline{s}\, p(\underline{\theta},\underline{x}-(\underline{x}\cdot\underline{\theta})\,\underline{\theta}-\underline{s})\,h(\underline{\theta},\underline{s}) \tag{17}$$

with

$$h(\underline{\theta},\underline{s}) = c\int_A d\underline{n}\, w(\underline{n})\,\delta(\underline{n}\cdot\underline{s})\,\delta(\underline{n}\cdot\underline{\theta})\,k_\mu(\underline{s}\cdot\underline{\alpha})\,, \quad \underline{s}\cdot\underline{\theta}=0\,. \tag{18}$$

Formula (17) is identical to (4) and (5). To get the expression (6) for $h(\underline{\theta},\underline{s})$, one must note that $\underline{s}=(\underline{s}\cdot\underline{\alpha})\,\underline{\alpha}$ in (18) because $\underline{s}\cdot\underline{\theta}=0$, $\underline{s}\cdot\underline{n}=0$ and $(\underline{\theta},\underline{n},\underline{\alpha})$ form an orthogonal basis in $\mathbb{R}^3$. Since k_μ is even, one can write

$$k_\mu(\underline{s}\cdot\underline{\alpha}) = k_\mu(|\underline{s}\cdot\underline{\alpha}|) = k_\mu(||\underline{s}||) \tag{19}$$

and thus

$$h(\underline{\theta},\underline{s}) = c\,\frac{k_\mu(||\underline{s}||)}{||\underline{s}||}\int_A d\underline{n}\, w(\underline{n})\,\delta(\underline{n}\cdot\frac{\underline{s}}{||\underline{s}||})\,\delta(\underline{n}\cdot\underline{\theta})\,, \quad \underline{s}\cdot\underline{\theta}=0 \tag{20}$$

which reduces to (6). (Recall that A is symmetric.)

The frequency-domain expression of the filter is obtained from (18) as follows

$$\begin{aligned} H(\underline{\theta},\underline{\nu}) &= \int_{\underline{s}\cdot\underline{\theta}=0} d\underline{s}\, e^{-j2\pi\underline{s}\cdot\underline{\nu}}\, h(\underline{\theta},\underline{s}) \\ &= c\int_{\underline{s}\cdot\underline{\theta}=0} d\underline{s}\, e^{-j2\pi\underline{s}\cdot\underline{\nu}} \int_A d\underline{n}\, w(\underline{n})\,\delta(\underline{n}\cdot\underline{s})\,\delta(\underline{n}\cdot\underline{\theta})\,k_\mu(\underline{s}\cdot\underline{\alpha}) \\ &= c\int_A d\underline{n}\, w(\underline{n})\,\delta(\underline{n}\cdot\underline{\theta}) \int_{\underline{s}\cdot\underline{\theta}=0} d\underline{s}\, e^{-j2\pi\underline{s}\cdot\underline{\nu}}\,\delta(\underline{n}\cdot\underline{s})\,k_\mu(\underline{s}\cdot\underline{\alpha}) \\ &= c\int_{\mathcal{C}(\underline{\theta})\cap A} d\underline{n}\, w(\underline{n}) \int_{\underline{s}\cdot\underline{\theta}=0} d\underline{s}\, e^{-j2\pi\underline{s}\cdot\underline{\nu}}\,\delta(\underline{n}\cdot\underline{s})\,k_\mu(\underline{s}\cdot\underline{\alpha})\,. \end{aligned} \tag{21}$$

Using $\underline{s}=u\,\underline{\alpha}+v\,\underline{\beta}$, with $\underline{\beta}=\underline{n}$, one gets

$$\begin{aligned} H(\underline{\theta},\underline{\nu}) = & \; c\int_{\mathcal{C}(\underline{\theta})\cap A} d\underline{n}\, w(\underline{n}) \\ & \int_{\mathbb{R}} du \int_{\mathbb{R}} dv\; e^{-j2\pi(u\,\underline{\nu}\cdot\underline{\alpha}+v\,\underline{\nu}\cdot\underline{\beta})}\,\delta(v)\,k_\mu(u) \\ = & \; c\int_{\mathcal{C}(\underline{\theta})\cap A} d\underline{n}\, w(\underline{n})\,K_\mu(\underline{\nu}\cdot\underline{\alpha}) \end{aligned} \tag{22}$$

where K_μ is the 1D Fourier transform of k_μ:

$$K_\mu(R) = \begin{cases} |R|/2 & \text{if } |R|>\mu_0/2\pi \\ 0 & \text{otherwise} \end{cases} \tag{23}$$

Inserting the definition of K_μ in (22), one obtains equation (9) since $\underline{\alpha}=\underline{n}\times\underline{\theta}$.

III. Specific geometries

In this section, we apply the A-TTR algorithm to specific geometries, namely the full sphere and the equatorial band.

It is worth mentionning that the full sphere case had been analyzed previously by Hazou [8] and Weng *et al.* [9]. Both papers proposed an FBP algorithm, but different approaches were used to solve the reconstruction problem. Weng *et al.* derived a spatial-domain convolution filter, while Hazou derived a frequency-domain filter. No links were established between the two algorithms. Below, we will see that the filter in the A-TTR algorithm with $w(\underline{n}) = 1$ is identical to the filter in [9] when expressed in the spatial domain and also identical to the filter in [8] when expressed in the Fourier domain. The FBP algorithms in [8] and [9] are therefore mathematically equivalent and can be expressed as particular cases of the A-TTR algorithm. As a consequence of this result, we observe that there is no need to resort to the approximation in [9] for the implementation of the algorithm since the convolution step can be accurately implemented from the knowledge of the Fourier transform of the filter, as described in section II.B.

On the other hand, this paper is the first work presenting a closed-form inversion formula for reconstruction from exponential X-ray projections sampled on an equatorial band.

A. The full sphere

In this section, Ω is the set of all possible unit vectors in $\mathbb{R}^3$. Mathematically, we write $\Omega = S^2$ where S^2 is the unit sphere:

$$S^2 = \left\{ \underline{\theta} \in \mathbb{R}^3 \ : ||\underline{\theta}|| = 1 \right\}. \tag{24}$$

In this particular case, one has $A = \Omega = S^2$. Therefore, the convolution filter (6) can be written in the form

$$h(\underline{\theta}, \underline{s}) = 2\,c\,\frac{k_\mu(||\underline{s}||)}{||\underline{s}||}\, w(\underline{\theta} \times \frac{\underline{s}}{||\underline{s}||}). \tag{25}$$

Taking $w(\underline{n}) = 1$ for all $\underline{n}$, which consists in equally weighting each projection, and using equation (8) for k_μ, one gets

$$\begin{aligned} h(\underline{\theta}, \underline{s}) = & \ \frac{1}{2\pi}\,\frac{k_\mu(||\underline{s}||)}{||\underline{s}||} \\ = & \ -\frac{\cos(\mu||\underline{s}||) + \mu||\underline{s}||\,\sin(\mu||\underline{s}||)}{8\pi^3\,||\underline{s}||^2}. \end{aligned} \tag{26}$$

since $c = 1/4\pi$ (see equation (7)). This filter expression was previously derived by Weng *et al.* [9].

Now, we calculate the frequency expression (9) of the A-TTR filter for $w(\underline{n}) = 1$. Recall first that $H(\underline{\theta}, \underline{\nu}) = 0$ when $||\underline{\nu}|| < \mu_0/2\pi$. Below, we consider that $||\underline{\nu}|| \geq \mu_0/2\pi$. Let $\underline{\alpha}$ and $\underline{\beta}$ be two unit orthogonal vectors perpendicular to $\underline{\theta}$ such that $\underline{\alpha} \times \underline{\beta} = \underline{\theta}$. Using these vectors, angles ω and ψ can be introduced to write

$$\begin{aligned} \underline{n} = & \ \cos\omega\,\underline{\alpha} + \sin\omega\,\underline{\beta}, \\ \underline{n} \times \underline{\theta} = & \ \sin\omega\,\underline{\alpha} - \cos\omega\,\underline{\beta}, \\ \underline{\nu} = & \ ||\underline{\nu}||\,(\cos\psi\,\underline{\alpha} + \sin\psi\,\underline{\beta}). \end{aligned} \tag{27}$$

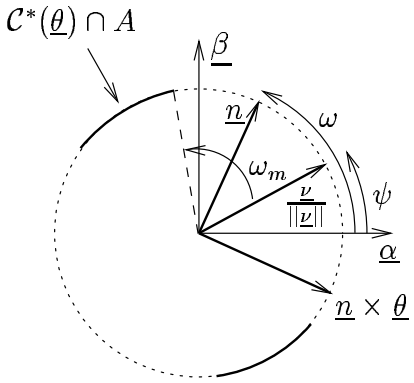

Fig. 3. Definition of angles ω and ψ and illustration of a possible ω_m value. The dark curve on the unit disk is the integration region (30).

See figure 3. These expressions lead to

$$\underline{\nu} \cdot (\underline{n} \times \underline{\theta}) = ||\underline{\nu}||\,\sin(\omega - \psi). \tag{28}$$

Define $\omega_m \in [0, \pi/2[$ such that

$$\sin\omega_m = \frac{\mu_0}{2\pi\,||\underline{\nu}||}. \tag{29}$$

Since $A = S^2$, one has

$$\begin{aligned} \mathcal{C}^*(\underline{\theta}) \cap A = & \ \mathcal{C}^*(\underline{\theta}) \\ = & \ \Big\{ \underline{n} = \cos\omega\,\underline{\alpha} + \sin\omega\,\underline{\beta} \ : \\ & \qquad |\sin(\omega - \psi)| > \sin\omega_m \Big\}. \end{aligned} \tag{30}$$

Therefore, with $w(\underline{n}) = 1$ and involving (7), (28), (29) and (30), one obtains $c = 1/4\pi$ and for $||\underline{\nu}|| \geq \mu_0/2\pi$

$$\begin{aligned} H(\underline{\theta}, \underline{\nu}) = & \ \frac{||\underline{\nu}||}{8\pi} \int_{|\sin(\omega-\psi)|>\sin\omega_m} d\omega\,|\sin(\omega - \psi)| \\ = & \ \frac{||\underline{\nu}||}{8\pi} \int_{|\sin(\omega)|>\sin\omega_m} d\omega\,|\sin(\omega)| \\ = & \ \frac{||\underline{\nu}||}{4\pi} \int_{\omega_m}^{\pi-\omega_m} d\omega\,\sin\omega \\ = & \ \frac{||\underline{\nu}||}{2\pi}\,\cos\omega_m \\ = & \ \frac{1}{2\pi}\sqrt{||\underline{\nu}||^2 - \frac{\mu_0^2}{4\pi^2}}. \end{aligned} \tag{31}$$

(Recall from equation (11) that $H(\underline{\theta}, \underline{\nu}) = 0$ for $||\underline{\nu}|| < \mu_0/2\pi$.) This filter expression was previously derived by Hazou [8]. The mathematical developments in section II.C prove that (31) is the Fourier transform of (26).

Note that the filter $H(\underline{\theta}, \underline{\nu})$ is here identical for all projection directions $\underline{\theta}$ because $w(\underline{n}) = 1$ was selected. Note also that $H(\underline{\theta}, \underline{\nu})$ is not dependent on the polar angle ψ of $\underline{\nu}$ (see equation (27)). Figure 4 compares the look of $H(\underline{\theta}, \underline{\nu})$ in the attenuated and non-attenuated cases. The part only for $\psi \in [0, \pi/2[$ is displayed.

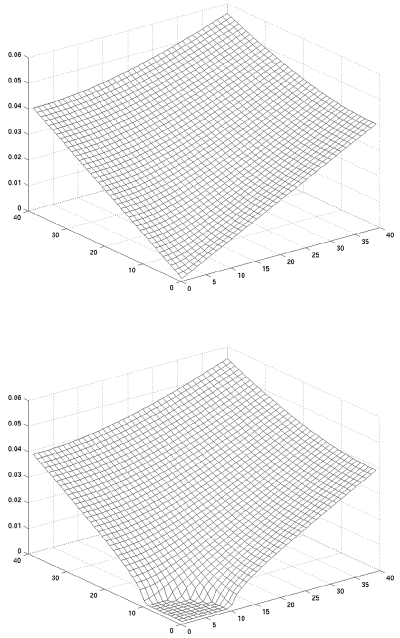

Fig. 4. Frequency-domain filter for the full sphere. Top: no attenuation. Bottom: with attenuation.

B. The equatorial band

In this section, Ω is the equatorial band of aperture θ_0 illustrated in figure 1a. Mathematically, we write

$$\Omega = \left\{ \underline{\theta} \in S^2 \ : \quad |\underline{\theta} \cdot \underline{e}_z| \leq \sin\theta_0 \right\}. \tag{32}$$

For this set, one has

$$A = \left\{ \underline{n} \in S^2 \ : \quad |\underline{n} \cdot \underline{e}_z| \geq \cos\theta_0 \right\}. \tag{33}$$

See figure 1b. Equation (33) with (6) specifies the spatial-domain expression of the A-TTR filter. Below, we give details on the calculation of the frequency-domain expression of the filter. For this calculation, $w(\underline{n}) = 1$ is assumed. That is

$$c = \frac{1}{4\pi\,(1-\cos\theta_0)} \tag{34}$$

(see equation (7)). Recall first that $H(\underline{\theta},\underline{\nu}) = 0$ when $||\underline{\nu}|| < \mu_0/2\pi$, i.e. $H(\underline{\theta},\underline{\nu})$ needs only to be calculated for $||\underline{\nu}|| \geq \mu_0/2\pi$. As in section III.A, we introduce unit orthogonal vectors $\underline{\alpha}$ and β such that $\underline{\alpha} \times \underline{\beta} = \underline{\theta}$. We also define angles ω and ψ such that

$$\begin{aligned} \underline{n} &= \cos\omega\,\underline{\alpha} + \sin\omega\,\underline{\beta}, \\ \underline{n} \times \underline{\theta} &= \sin\omega\,\underline{\alpha} - \cos\omega\,\underline{\beta}, \\ \underline{\nu} &= ||\underline{\nu}||\,(\cos\psi\,\underline{\alpha} + \sin\psi\,\underline{\beta}). \end{aligned} \tag{35}$$

With these notations, one has as before

$$\underline{\nu} \cdot (\underline{n} \times \underline{\theta}) = ||\underline{\nu}||\,\sin(\omega - \psi) \tag{36}$$

and

$$\mathcal{C}^*(\underline{\theta}) = \left\{ \underline{n} = \cos\omega\,\underline{\alpha} + \sin\omega\,\underline{\beta} \ : \quad |\sin(\omega-\psi)| > \sin\omega_m \right\}. \tag{37}$$

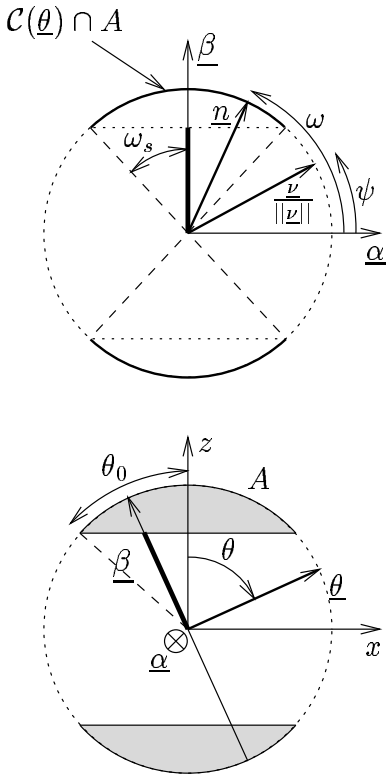

Fig. 5. Top: Description of the set $\mathcal{C}(\underline{\theta}) \cap A$. Bottom: Intersection of the unit sphere with the plane $(\underline{\theta},\underline{\beta})$. In both figures the dark segment of line has the same length. Expressing that condition leads to equation (40) for ω_s.

where

$$\sin\omega_m = \frac{\mu_0}{2\pi\,||\underline{\nu}||}. \tag{38}$$

To carry out the calculation of $H(\underline{\theta},\underline{\nu})$ according to formulas (9) and (10), note that

$$\mathcal{C}^*(\underline{\theta}) \cap A = \mathcal{C}^*(\underline{\theta}) \cap \left(\mathcal{C}(\underline{\theta}) \cap A \right). \tag{39}$$

Figure 5(top) illustrates the region $\mathcal{C}(\underline{\theta}) \cap A$. This region consists of two arcs of aperture $2\omega_s$ diametrically opposed. It is convenient to select the vectors $\underline{\alpha}$ and $\underline{\beta}$ to be the symmetry axes of $\mathcal{C}(\underline{\theta}) \cap A$ as shown in figure 5(top). The angle ω_s is defined by

$$\cos\omega_s = \frac{\cos\theta_0}{\sin\theta} \tag{40}$$

where θ is the polar angle of $\underline{\theta}$. See figure 5(bottom). Mathematically, one has

$$\mathcal{C}(\underline{\theta}) \cap A = \left\{ \underline{n} = \cos\omega\,\underline{\alpha} + \sin\omega\,\underline{\beta} \ : \quad |\sin\omega| > \cos\omega_s \right\}. \tag{41}$$

Therefore, involving equations (36), (37) and (41), one finds

$$H(\underline{\theta},\underline{\nu}) = \frac{||\underline{\nu}||}{8\pi\,(1-\cos\theta_0)} \int_W d\omega\,|\sin(\omega-\psi)| \tag{42}$$

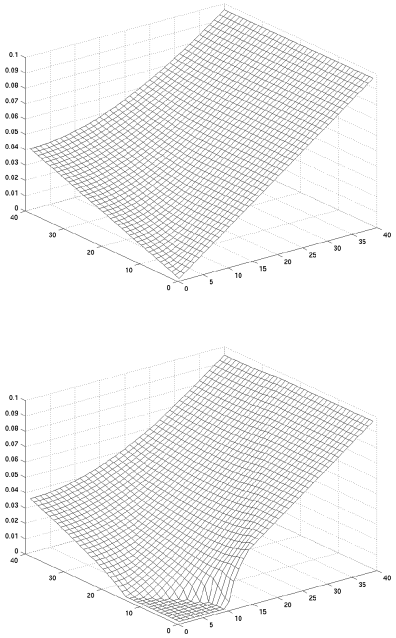

Fig. 6. Frequency-domain filter for the equatorial band - $\theta = 90°$. Top: no attenuation. Bottom: with attenuation.

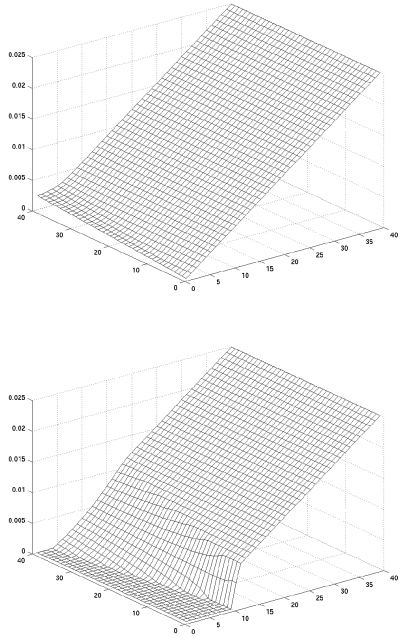

Fig. 7. Frequency-domain filter for the equatorial band - $\theta = 46°$. Top: no attenuation. Bottom: with attenuation.

where

$$W = \left\{ \omega \in [0, 2\pi[: \quad \begin{array}{c} |\sin(\omega - \psi)| \geq \sin \omega_m \,, \\ |\sin \omega| > \cos \omega_s \end{array} \right\}. \quad (43)$$

Or, equivalently

$$H(\underline{\theta}, \underline{\nu}) = \frac{||\underline{\nu}||}{8\pi \, (1 - \cos \theta_0)} \int_{W'} d\omega' \, |\sin \omega'| \quad (44)$$

where

$$W' = \left\{ \omega' \in [0, 2\pi[: \quad \begin{array}{c} |\sin \omega'| \geq \sin \omega_m \,, \\ |\sin(\omega' + \psi)| > \cos \omega_s \end{array} \right\}. \quad (45)$$

From these last two equations, one can easily check that $H(\underline{\theta}, \underline{\nu})$ needs only to be known for $\psi \in [0, \pi/2[$ because replacing ψ by $-\psi$ or $\psi + \pi$ does not change the filter expression. Straightforward (but tedious) calculation of the integral in (44) leads to the expression given in table 1 for $H(\underline{\theta}, \underline{\nu})$.

Note that the filter $H(\underline{\theta}, \underline{\nu})$ is here identical for directions $\underline{\theta}$ which have the same polar angle θ but different azimuthal angles. This is because $w(\underline{n}) = 1$ was selected and Ω is symmetric about the z-axis. Figure 6 and 7 compare the look of $H(\underline{\theta}, \underline{\nu})$ in the attenuated and non-attenuated cases for $\theta = 90°$ and $\theta = 46°$ respectively, when the aperture $\theta_0 = 45°$. In each case, only the part $\psi \in [0, \pi/2[$ is displayed. The expression of the filter in the non-attenuated case can be found in [12] or by taking the limit for μ_0 tending to zero in the expression of the A-TTR filter.

Figure 8 shows the reconstruction of a simulated phantom modelling the heart. This phantom consists of three ellipsoids, two of which model the ventricules with 20%

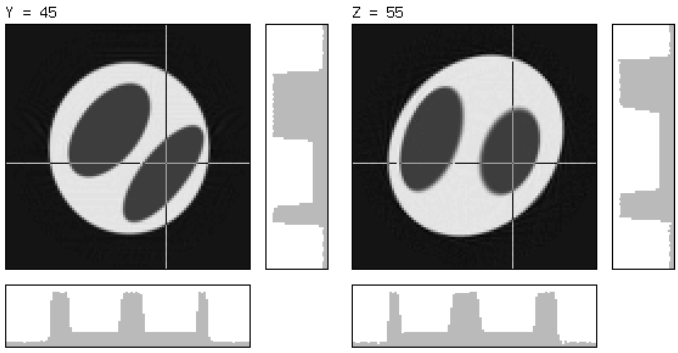

Fig. 8. Equatorial band. Reconstruction of a simulated phantom of the heart for $\theta_0 = 45$ degrees and $\mu_0 = 0.0152\, mm^{-1}$. Left: vertical slice. Right: horizontal slice.

of activity. The reconstruction was achieved on a grid of 100^3 cubic voxels of side 1.5 mm, using $\theta_0 = 45°$ and $\mu_0 = 0.0152$ mm^{-1}. The set Ω was uniformly sampled in spherical coordinates with a step of 3 degrees and the projections were sampled on grids of 128^2 pixels of side 1.5 mm. The quality of the reconstruction in figure 8 demonstrates the exactness of the algorithm.

IV. Conclusions and discussion

We have shown that a closed-form inversion formula can be derived for 3-D image reconstruction from exponential X-ray projections sampled on any subset of the unit sphere that includes great circles.

The new algorithm, called the A-TTR algorithm, is of FBP type. It has the particularity of dealing only with

$G(\psi,\omega_m)$		$\omega_m < \omega_s$	$\omega_m \geq \omega_s$
$\psi < \frac{\pi}{2} - \omega_s - \omega_m$	$\frac{\pi}{2} + \omega_s < \pi + \psi - \omega_m$	$4 \sin\omega_s \cos\psi$	
	$\frac{\pi}{2} + \omega_s \geq \pi + \psi - \omega_m$	$2\cos\omega_m + 2\sin\omega_s\cos\psi + 2\sin\psi\cos\omega_s$	
$\frac{\pi}{2} - \omega_s - \omega_m \leq \psi < \frac{\pi}{2} - \lvert\omega_s - \omega_m\rvert$	$\frac{\pi}{2} + \omega_s < \pi + \psi - \omega_m$	$2\cos\omega_m + 2\sin\omega_s\cos\psi - 2\sin\psi\cos\omega_s$	
	$\frac{\pi}{2} + \omega_s \geq \pi + \psi - \omega_m$	$4\cos\omega_m$	
$\frac{\pi}{2} - \lvert\omega_s - \omega_m\rvert \leq \psi < \frac{\pi}{2}$		$4\cos\omega_m - 4\sin\psi\cos\omega_s$	0

TABLE I

Frequency-domain expression of the A-TTR filter for the equatorial band. The filter is expressed in the form $H(\underline{\theta},\underline{\nu}) = G(\psi,\omega_m)\,||\underline{\nu}||/8\pi(1-\cos\theta_0)$. The table gives the values of $G(\psi,\omega_m)$ according to the values taken by ψ, ω_s and ω_m. The vector $\underline{\nu} = ||\underline{\nu}||\,(\cos\psi\,\underline{\alpha} + \sin\psi\,\underline{\beta})$. The table should be used only for $\psi \in [0, \pi/2[$ and $||\underline{\nu}|| \geq \mu_0/2\pi$. For $||\underline{\nu}|| < \mu_0/2\pi$, $H(\underline{\theta},\underline{\nu}) = 0$. The dependence of $H(\underline{\theta},\underline{\nu})$ on $\underline{\theta}$ is burried in the definition of ω_s (see equation (40)).

projections that are on great circles in Ω. Projections that are not on great circles are not used in the A-TTR reconstruction. This is due to the way the algorithm was derived. At this stage of our research, we do not know if filters involving all measurements in Ω can be designed for exact FBP reconstruction. Further investigations are also required for reconstruction from data sets that do not include great circles but may contain enough information for exact reconstruction.

The A-TTR algorithm was applied to two specific geometries: the full sphere and the equatorial band. The results for the full sphere showed that the algorithms previously proposed by Hazou [8] and Wang *et al.* [9] are mathematically identical. The results for the equatorial band were original.

The noise properties of the algorithm were not analyzed in this paper. From existing results in 2-D [6][7], it is however reasonable to think that the A-TTR algorithm does not handle noise in an optimal way. As in the 2-D case, it is likely that the exponential weight in the backprojection step excessively amplifies the noise, especially at the periphery of the reconstructed image. Further work is required for the development of inversion formulas which handle noise in an optimal way similar to the 2-D method developed in [6][7].

Acknowledgements

The work of F. Noo was supported by the Belgian National Fund for Scientific Research. The authors thank Michel Defrise from the Free University of Brussels for stimulating discussions.

References

[1] M. Braunstein and R. Y. Levine, "Optimum beam configurations in tomographic intensity modulated radiation therapy", *Phys. Med. Biol.*, Vol. 45, 305-328, 2000.

[2] S. J Glick, B. C. Penney, M. A. King and C. L. Byrne, "Noniterative compensation for the distance-dependent detector response and photon attenuation in SPECT imaging", *IEEE Trans. Med. Imag.*, vol. 13(2), 363-374, 1994.

[3] X. Pan and C. E. Metz, "Analytical approaches for image reconstruction in 3D SPECT", *in Three-dimensional Image Reconstruction in Radiation and Nuclear Medicine*, ed. P.Grangeat and J.-L. Amans (Dordrecht: Kluwer), 103-115, 1996.

[4] C. Mennessier, F. Noo, R. Clack, G. Bal and L. Desbat, "Attenuation correction in SPECT using consistency conditions for the exponential ray transform", *Phys. Med. Biol.*, Vol 44, 2483-2510, 1999.

[5] R. Clack, P. E. Christian, M. Defrise and A. E. Welch, "Image reconstruction for a novel SPECT system with rotating slant-hole collimators". *In Conf. Rec. 1995 IEEE Med. Imag.* Conf., 1948-1952, 1996.

[6] C. E. Metz and X. Pan, "A unified analysis of exact methods of inverting the 2D exponential Radon transform, with implications for Noise Control in SPECT", *IEEE Trans. Med. Imag.*, vol. 14(4), 1995.

[7] X. Pan and C. E. Metz, "Analysis of noise properties of a class of exact methods of inverting the 2D exponential Radon transform", *IEEE Trans. Med. Imag.*, vol. 14(4), 1995.

[8] I. A. Hazou, "Inversion of the exponential X-ray transform. I: Analysis", *Math. Methods in the Applied Sciences*, Vol. 10(10), 561-574 (1988).

[9] Y. Weng, G. L. Zeng and G. T. Gullberg, "Filtered backprojection algorithms for attenuated parallel and cone-beam projections sampled on a sphere", *in Three-dimensional Image Reconstruction in Radiation and Nuclear Medicine*, ed. P.Grangeat and J.-L. Amans (Dordrecht: Kluwer), 19-34, 1996.

[10] S. S. Orlov, "Theory of three dimensional reconstruction. 1. Conditions of a complete set of projections.", *Sov. Phys.-Crystallogr., Vol. 20, 312-314, 1975.*

[11] M. Defrise, D. W. Townsend and R. Clack, "Three-dimensional image reconstruction from complete projections", *Phys. Med. Biol.*, Vol. 34(5), 573-587, 1989.

[12] J. B. Ra, C. B. Lim, Z. H. Cho, S. K. Hilal and J. Correll "A true three-dimensional reconstruction algorithm for the spherical positron emission tomograph", *Phys. Med. Biol.*, Vol. 27, 37-50, 1982.

[13] A. Markoe, "Fourier inversion of the attenuated X-ray transform", *SIAM J. Math. Anal.*, Vol. 15(4), 718-722, 1984.

[14] O. Tretiak and C. Metz, "The exponential Radon transform", *SIAM J. Appl. Math.*, Vol. 39(2), 341-354, 1980.